Rapid Communications

Structure formation models weaken limits on WIMP dark matter from dwarf spheroidal galaxies

Shin'ichiro Ando,[1,2,*] Alex Geringer-Sameth,[3,4] Nagisa Hiroshima,[5,6,7] Sebastian Hoof,[8] Roberto Trotta,[3,9,10] and Matthew G. Walker[11]

[1]*GRAPPA Institute, University of Amsterdam, 1098 XH Amsterdam, Netherlands*
[2]*Kavli Institute for the Physics and Mathematics of the Universe (Kavli IPMU, WPI), University of Tokyo, Kashiwa, Chiba 277-8583, Japan*
[3]*Department of Physics, Imperial College London, London SW7 2AZ, United Kingdom*
[4]*Department of Mathematics, Imperial College London, London SW7 2AZ, United Kingdom*
[5]*RIKEN Interdisciplinary Theoretical and Mathematical Sciences (iTHEMS), Wako, Saitama 351-0198, Japan*
[6]*Department of Physics, University of Toyama, Toyama 930-8555, Japan*
[7]*Institute of Particle and Nuclear Studies, High Energy Accelerator Research Organization (KEK), Tsukuba, Ibaraki 305-0801, Japan*
[8]*Institut für Astrophysik, Georg-August Universität, Friedrich-Hund-Platz 1, 37077 Göttingen, Germany*
[9]*Data Science Institute, William Penney Laboratory, Imperial College London, London SW7 2AZ, United Kingdom*
[10]*SISSA, Physics Department, Via Bonomea 265, 34136 Trieste, Italy*
[11]*McWilliams Center for Cosmology, Department of Physics, Carnegie Mellon University, Pittsburgh, Pennsylvania 15213, USA*

(Received 2 March 2020; revised 4 May 2020; accepted 25 August 2020; published 17 September 2020)

Dwarf spheroidal galaxies that form in halo substructures provide stringent constraints on dark matter annihilation. Many *ultrafaint* dwarfs discovered with modern surveys contribute significantly to these constraints. At present, because of the lack of abundant stellar kinematic data for the ultrafaints, noninformative prior assumptions are usually made for the parameters of the density profiles. Based on semianalytic models of dark matter subhalos and their connection to satellite galaxies, we present more informative and realistic *satellite priors*. We show that our satellite priors lead to constraints on the annihilation rate that are between a factor of 2 and a factor of 7 *weaker* than under noninformative priors. As a result, the thermal relic cross section can at best only be excluded (with 95% probability) for dark matter masses of $\lesssim$40 GeV from dwarf spheroidal data, assuming annihilation into $b\bar{b}$.

DOI: 10.1103/PhysRevD.102.061302

I. INTRODUCTION

The search to uncover the nature of dark matter is one of the greatest challenges in modern physics. If dark matter is made of weakly interacting massive particles (WIMPs), as motivated by the thermal freezeout argument [1,2] or supersymmetry [3], it can self-annihilate, producing observable gamma rays.

Dwarf spheroidal galaxies (dSphs) are associated with dark matter substructure (or subhalos). Given their proximity to us and paucity of baryons—and hence relative lack of astrophysical backgrounds—they offer the most robust environments to test the WIMP hypothesis [4–6]. In recent years, many new *ultrafaint* dSphs have been found [7]. While the small baryonic content of ultrafaint dSphs makes them promising targets for WIMP searches, the resulting dearth of stars makes it difficult to estimate their density profiles from dynamical analyses of kinematic data. A Bayesian approach can help by including additional, physical information on the parameters describing the dark matter density profile (such as a scale radius r_s and a characteristic density ρ_s [8]) in the form of prior probability distribution functions (PDFs). The literature to date [e.g., [9–12]] has usually adopted "uninformative" *uniform priors* for both $\log r_s$ and $\log \rho_s$ (see Ref. [13] for an alternative Bayesian hierarchical analysis and Refs. [14,15] for frequentist analyses of classical dSphs). However, such uniform priors ignore theoretical and numerical simulation results that predict the frequency distributions of subhalo parameters in the standard cold dark matter framework. While it may be appropriate to adopt such uniform priors when allowing for a variety of dark matter models, when testing WIMP dark matter specifically it is more appropriate to adopt priors derived from that model. (See Ref. [16] for a theoretical approach adopting the r_s-ρ_s

*s.ando@uva.nl

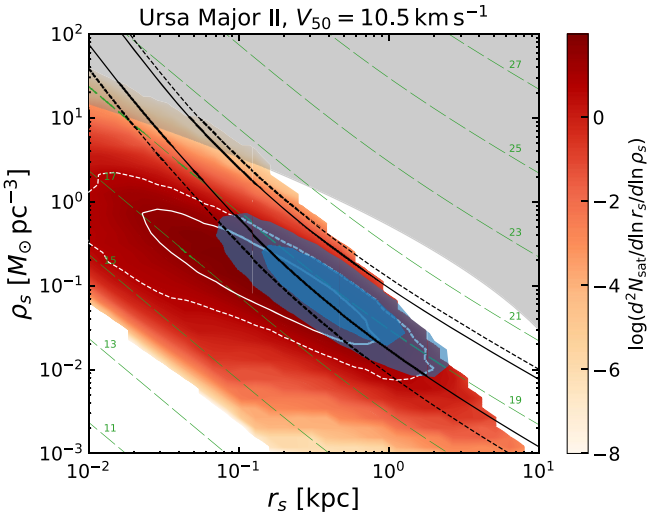

FIG. 1. Prior and posterior distributions in (r_s, ρ_s) parameter space for Ursa Major II. The red color map represents the satellite number density with $V_{50} = 10.5\ \mathrm{km\,s^{-1}}$ [cf. Eq. (2)]: $d^2N_{\rm sat}/(d\ \ln\ r_s d\ \ln\ \rho_s)$. The open white, open black, and filled blue contours show 68% and 95% confidence/credible regions of priors, likelihood, and posteriors, respectively. The gray shaded region is the GS15 cut, excluded in previous work [10]. The green dashed curves correspond to constant values of $\log[J(0.5°)/(\mathrm{GeV^2\,cm^{-5}})]$, indicated alongside.

correlation expected for field halos based on a concentration-mass relation [17].) For classical dSphs with well-measured velocity dispersion profiles, the adopted priors are relatively unimportant, as the inference is dominated by the data. Therefore, we focus on the ultrafaint dSphs, where the data are sparse and a physically motivated prior becomes critical. Including structure-formation physics in the prior represents a major improvement compared to the approaches adopted to date, which use uninformative priors or are otherwise "data-driven," thus neglecting relevant physical information.

As we show in this work, subhalos occupy only specific regions of the parameter space (see the red color map in Fig. 1). Realistic constraints on WIMP annihilation, therefore, should use an informative prior distribution based on our best understanding of how dwarf galaxies form in subhalos. Such a prior is difficult to generate from N-body simulations, because of the limited statistics of relatively large subhalos that can host dSphs. In this paper, we construct realistic *satellite priors* for the relevant parameters of the ultrafaint dSphs' dark matter distributions by using semianalytic models based on the extended Press-Schechter (EPS) formalism combined with tidal effects on subhalo evolution, as developed in Refs. [18–20] (see also [21,22]). We apply these novel satellite priors to obtain more realistic estimates of the gamma-ray flux from WIMP annihilation in dSphs. This results in a significant reduction of the predicted gamma-ray flux from ultrafaint dSphs compared with previous studies [9–15,23–38].

II. ASTROPHYSICAL J FACTOR

The gamma-ray flux from dark matter self-annihilation from each dSph is proportional to the so-called astrophysical J factor, defined as

$$J(\alpha_{\rm int}) = 2\pi \int_0^{\alpha_{\rm int}} d\psi\ \sin\psi \int dl \rho^2(r[l,\psi]), \qquad (1)$$

where ψ is the angle relative to the direction toward the center of the dSph, $\alpha_{\rm int}$ is the radius of the integration aperture, $\rho(r)$ is the dark matter density, $r^2 = l^2 + D^2\sin^2\psi$, l is line of sight distance from Earth, and D is the distance to the dSph. It is commonly assumed that the density profile $\rho(r)$ is given by a spherically symmetric function, such as the Navarro-Frenk-White (NFW) profile [8], $\rho(r) = \rho_s r_s^3/[r(r+r_s)]$, out to a tidal truncation radius r_t (but see also Refs. [12,28] for axisymmetric profiles).

III. SUBHALO MODELS

In order to determine physically motivated priors, we adopt the semianalytic models of subhalos developed in Refs. [19,20]. We focus on a host halo with mass $M = 10^{12}\ M_\odot$ at redshift $z = 0$. The differential number of smaller halos with mass m_a that accreted onto the host at redshift z_a (and henceforth become subhalos), $d^2N_{\rm sh}/(dm_a dz_a)$, is described with the EPS formalism [39], calibrated against numerical simulations [40]. After accretion, we model the evolution of the density profiles of the subhalos, which are well approximated by truncated NFW profiles [41], by taking tidal effects into account [42,43]. This procedure predicts the distribution of subhalo variables at $z = 0$. The relevant variables for the J factor are r_s, ρ_s, and r_t, whose joint probability density is proportional to the abundance of subhalos: $P_{\rm sh}(r_s, \rho_s, r_t) \propto d^3N_{\rm sh}/(dr_s d\rho_s dr_t)$. In the Supplemental Material (SM) [44], we show that the ensuing distribution of r_s and ρ_s is in excellent agreement with the results from numerical simulations, as is the associated subhalo mass function [19].

IV. SUBHALO-SATELLITE CONNECTION

In order to connect the subhalo population to that of the dSphs that form within them, we adopt the simple prescription given in Ref. [45]. The probability that a satellite galaxy forms in a host subhalo is given by

$$P_{\rm form}(V_{\rm peak}) = \frac{1}{2}\left[1 + \mathrm{erf}\left(\frac{V_{\rm peak} - V_{50}}{\sqrt{2}\sigma}\right)\right], \qquad (2)$$

where $V_{\rm peak}$ is the peak value of the maximum circular velocity of the satellite, V_{50} is where $P_{\rm form}$ is $1/2$, and we adopt $\sigma = 2.5\ \mathrm{km\,s^{-1}}$, following Ref. [45]. (See Ref. [46] for different criteria related to reionization.)

In our model, $V_{\rm peak}$ is obtained at the time the subhalo accretes onto its host, i.e., $V_{\rm peak} = (4\pi G\rho_{s,a}/4.625)^{1/2} r_{s,a}$, where $\rho_{s,a}$ and $r_{s,a}$ are determined at accretion (see SM [44]). According to the conventional theory of galaxy formation, we adopt a value of V_{50} that allows atomic cooling to form galaxies in subhalos: $V_{50} = 18\ {\rm km\,s^{-1}}$. However, Ref. [45] found that $V_{50} = 18\ {\rm km\,s^{-1}}$ underpredicts the number of dSphs and their radial distribution compared with the observations, and suggested smaller values. Thus, we also adopt $V_{50} = 10.5\ {\rm km\,s^{-1}}$ [45].

V. SATELLITE PRIOR

From the above distribution for subhalos we derive a distribution for satellite galaxies, which we then adopt as a prior in the analysis of kinematic data from each observed galaxy. When analyzing kinematic data, the dark matter profile of each satellite is described by parameters (r_s, ρ_s, r_t). Our model results in a prior PDF:

$$P_{\rm sat}(r_s,\rho_s,r_t) \propto \frac{d^3N_{\rm sat}}{dr_s d\rho_s dr_t} = \frac{d^3N_{\rm sh}}{dr_s d\rho_s dr_t} P_{\rm form}(V_{\rm peak}). \quad (3)$$

The interpretation of this prior is that it assigns to each ultrafaint dSph an equal probability of being found in any subhalo that hosts a satellite galaxy.[1] The red color map in Fig. 1 shows the number density of satellites $d^2N_{\rm sat}/(d\ln r_s d\ln\rho_s)$ (after marginalization over r_t) for the case $V_{50} = 10.5\ {\rm km\,s^{-1}}$, while the white contours show 68% and 95% highest density credible regions.

Previous studies have used uniform priors in the $(\log r_s, \log\rho_s)$ parameter space with a sharp cut-off obtained from cosmological arguments for subhalo formation. For example, Ref. [10] uses the EPS formalism to evaluate the probability that the Milky Way hosts a subhalo with a given mass and collapse redshift and excludes parts of subhalo parameter space where this probability is low. This unphysical region is represented by the gray region in Fig. 1 and is referred to in what follows as the "GS15 cut" (see also Ref. [11]). Our model effectively allows us to replace this cut-off with a smooth transition.

VI. LIKELIHOOD FUNCTION FOR OBSERVED DWARF SPHEROIDALS

For each ultrafaint dSph, we take the data $\boldsymbol{d}$ to be summarized by the observed line-of-sight velocity dispersion $\hat\sigma_{\rm los}$, the angular projected half-light radius $\hat\theta_h$, and distance $\hat D$, while the true values of these quantities are written without hats. We assume the likelihood, i.e., the probability of obtaining data $\boldsymbol{d}$ for a dSph given model parameters $\boldsymbol{\theta}$, $P(\boldsymbol{d}|\boldsymbol{\theta}) \equiv \mathcal{L}(\boldsymbol{\theta})$, to be

$$\mathcal{L}(\boldsymbol{\theta}) = \prod_{x\in\{\theta_h,\sigma_{\rm los},D\}} \frac{1}{\sqrt{2\pi\sigma_x^2}} \exp\left[-\frac{(\hat x - x)^2}{2\sigma_x^2}\right], \quad (4)$$

where σ_x is the measurement uncertainty on $\hat x$ and x is the model value. For classical dSphs, velocity dispersion profiles provide additional important information but for the sparsely observed ultrafaints there is little to be gained in using more than the single value $\hat\sigma_{\rm los}$. Our data are detailed in the SM [44].

According to the virial theorem, for a spherical system in dynamic equilibrium, the line-of-sight velocity dispersion is given by [52]

$$\sigma_{\rm los}^2 = \frac{4\pi G}{3}\int_0^\infty dr\, r\nu_\star(r) M(r), \quad (5)$$

where $M(r)$ is the enclosed mass within radius r (assumed dominated by dark matter) and $\nu_\star(r)$ is the stellar density profile, for which we adopt a Plummer sphere: $\nu_\star(r) = 3[1+(r/R_h)^2]^{-5/2}/(4\pi R_h^3)$ with $R_h = D\theta_h$. For a subhalo characterized by $\boldsymbol{\theta} = (r_s, \rho_s, r_t, \theta_h, D)$, we compute $\sigma_{\rm los}$ with Eq. (5) and use this in Eq. (4) to evaluate the likelihood.

VII. POSTERIOR DISTRIBUTION

Applying Bayes' theorem using the satellite prior [Eq. (3)] and the likelihood [Eq. (4)], we obtain the posterior PDF of the subhalo quantities $\boldsymbol{\theta}$ as $P(\boldsymbol{\theta}|\boldsymbol{d}) \propto P_{\rm sat}(\boldsymbol{\theta})\mathcal{L}(\boldsymbol{\theta})$. In Fig. 1, we show the marginal posterior PDF on r_s and ρ_s for Ursa Major II as filled blue contours encompassing 68% and 95% probability (highest probability density regions), while the likelihood (maximized over θ_h and r_t, assuming $r_t \gg R_h$) is shown by the black contours. For log-uniform priors on r_s and ρ_s, the posterior would trace these iso-likelihood contours. The degeneracy between r_s and ρ_s, which occurs for ultrafaint dwarfs, can be broken by the additional information supplied by the prior.

Given values for r_s, ρ_s, and r_t, as well as distance D for each dSph, we evaluate $J(0.5°)$ [30]. In Fig. 1, we show contours of constant $\log[J/({\rm GeV^2\,cm^{-5}})]$ for Ursa Major II, from which one can see the impact of adopting different priors (log in this work is base-10). We ignore substructure boosts of the annihilation rate for dSphs, as they are at most a few tens of percent (see SM [44]). In addition, we ignore the errors on D (i.e., set $\sigma_D = 0$). The fractional errors in distance are much smaller than those on $\sigma_{\rm los}$ and we have checked that ignoring them has no impact on our results. The priors on θ_h and $\sigma_{\rm los}$ are uniform over positive values.

In Fig. 2, we show the marginalized posterior distribution on $\log J(0.5°)$ of Ursa Major II for four different priors. Compared with a log-uniform prior, the satellite prior

[1]The framework could be extended by adopting stellar-mass–halo-mass relations [47–50] as an additional factor in the likelihood. But these relations are known to have large uncertainty for faint galaxies [51], and we choose not to include them.

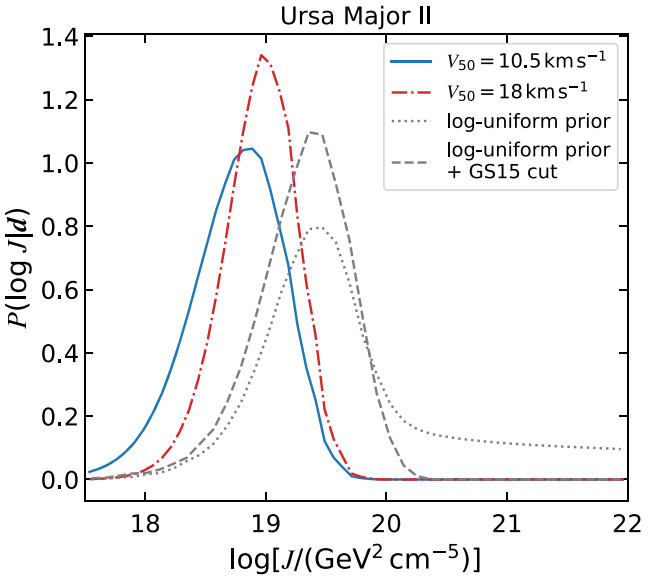

FIG. 2. Posterior distributions of $J(0.5°)$ for Ursa Major II, obtained with log-uniform priors for r_s and ρ_s (dotted), log-uniform priors with the GS15 cut that corresponds to the gray shaded region in Fig. 1 (dashed), satellite priors with $V_{50} = 18\ \mathrm{km\,s^{-1}}$ (dot-dashed), and $V_{50} = 10.5\ \mathrm{km\,s^{-1}}$ (solid). Median and 1σ credible regions for $\log[J/(\mathrm{GeV^2\,cm^{-5}})]$ from these posteriors are $19.58^{+1.54}_{-0.51}$, $19.34^{+0.34}_{-0.41}$, $18.96^{+0.28}_{-0.32}$, and $18.78^{+0.35}_{-0.42}$, respectively.

moves the posterior toward the bottom-left corner in (r_s, ρ_s) parameter space, which yields systematically smaller J factors. In the case of $V_{50} = 10.5\ \mathrm{km\,s^{-1}}$ ($18\ \mathrm{km\,s^{-1}}$), the median of the J distributions with the satellite prior is 3.6 (2.4) times smaller than when using a log-uniform prior with GS15 cut. We discuss all the other ultrafaints in the SM [44].

Figure 3 summarizes the median values and 68% and 95% credible intervals for $J(0.5°)$ for all ultrafaint dSphs (and the classical dSph Sagittarius, which we find has one of the largest J factor but has been considered in very few previous studies). The figure compares the results when using the satellite prior with different assumptions for V_{peak} to the results using log-uniform priors with the GS15 cut. We find that for ultrafaint dSphs exhibiting the largest J factors in previous analyses, adopting the satellite prior produces J distributions whose medians are systematically smaller. This generic result also holds true in comparison with earlier work [10,11,33]. In Fig. 3, we also show the J factors resulting from replacing the probability of a satellite forming in a host subhalo, Eq. (2), by a step function $P_{\mathrm{form}} = \Theta(V_{\mathrm{peak}} - V^{\mathrm{th}}_{\mathrm{peak}})$ with $V^{\mathrm{th}}_{\mathrm{peak}} = 6\ \mathrm{km\,s^{-1}}$. Although it may seem implausible that such small subhalos host galaxies in strong radiation fields after cosmic reionization, such a scenario has been suggested from the observed numbers and distribution of satellites [45]. In this extreme

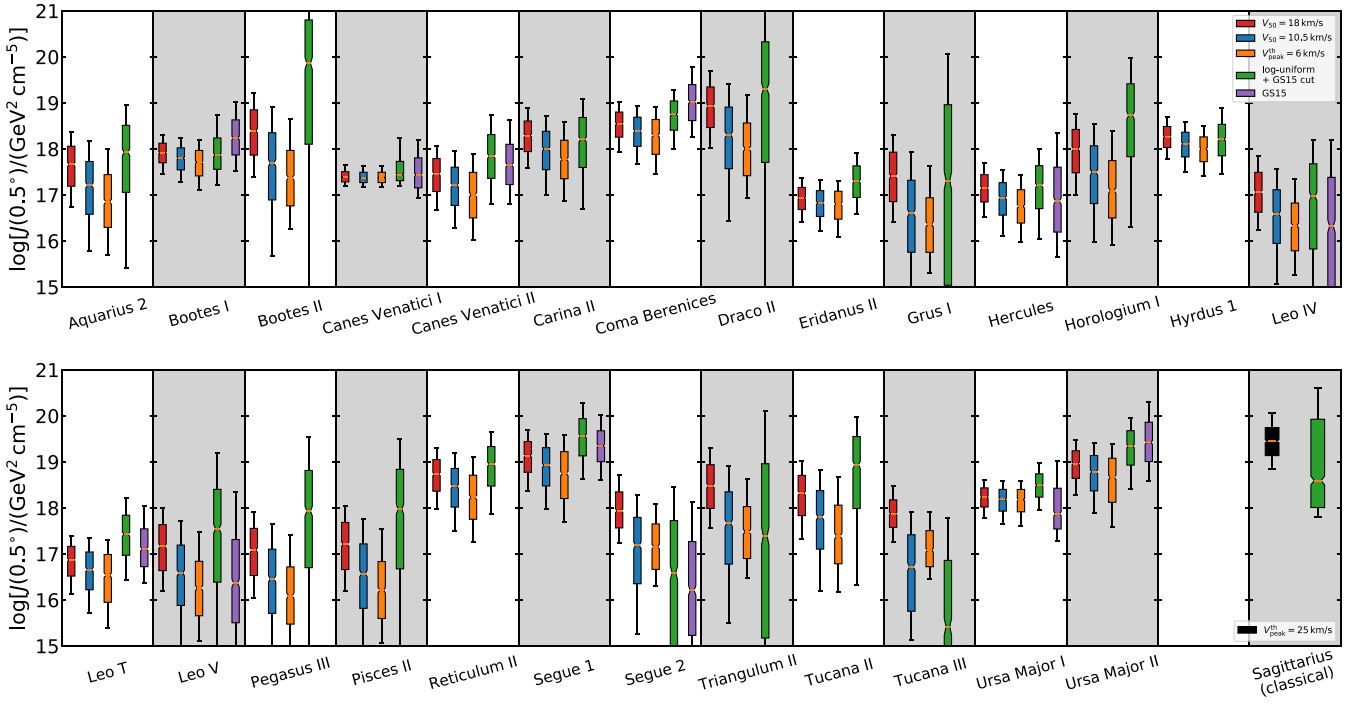

FIG. 3. Box-whisker diagram showing median values and equal-tailed 68% (boxes) and 95% (whiskers) credible intervals of the $J(0.5°)$ posteriors. For comparison, posteriors with priors uniform in $(\log r_s, \log \rho_s)$ with the GS15 cut and previous results from Ref. [10] are shown. The classical dSph Sagittarius uses a different satellite formation threshold of $V^{\mathrm{th}}_{\mathrm{peak}} = 25\ \mathrm{km\,s^{-1}}$ [46] (see SM [44] for the other classical dSphs).

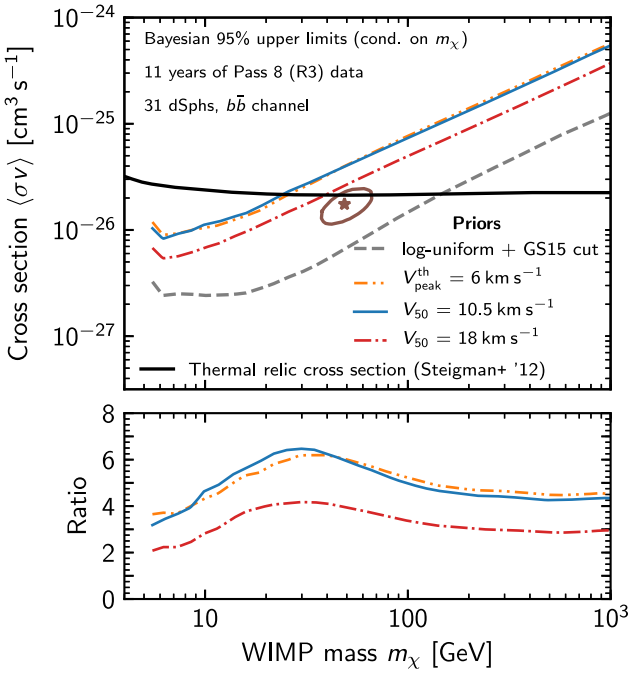

FIG. 4. Limits on the WIMP annihilation cross section $\langle\sigma v\rangle$ ($b\bar{b}$ channel) for different prior choices. Top: upper limits at 95% credibility (conditioned on the WIMP mass m_χ). The star and surrounding region indicate the parameter point and 2σ confidence levels associated with a possible Galactic centre excess [56] (see also [57–62]), respectively. Bottom: ratios of the cross-section upper limits obtained with satellite priors and those with log-uniform prior with GS15 cut; i.e., how much *weaker* the limits derived from the satellite priors are.

case, we observe that the J factor distributions shift even further toward smaller values.

VIII. CONSTRAINTS ON WIMP ANNIHILATION

We now quantify the impact of the satellite priors on annihilation cross section limits using Fermi-LAT gamma-ray data. We use a sample of 31 dSphs, adding Boötes II, Segue 2, Triangulum II, and Tucana III to the 27 dSphs in Ref. [35]. We do not include Sagittarius due to its proximity to the Galactic plane. Our data selection, background modeling and sampling techniques are as in Ref. [35]: we use around 11 years of Pass 8 (R3) data [53] in conjunction with the 4FGL source catalogue [54].

For the classical dSphs,[2] we use the J factor posteriors of Ref. [33] as priors in our analysis since J factors of classical dSphs are well-constrained by the large number of member stars and are relatively insensitive to the choice of prior distribution. For the ultrafaint dwarfs, we compute marginal J factor distributions under the following priors:

(i) Uniform prior on $(\log r_s, \log \rho_s)$ with the GS15 cut;
(ii) Satellite prior, Eq. (3), $V_{50} = 18$ km s^{-1};
(iii) Satellite prior, Eq. (3), $V_{50} = 10.5$ km s^{-1};
(iv) Satellite prior, Eq. (3), step function replacing Eq. (2), $V_{\rm peak}^{\rm th} = 6$ km s^{-1}.

We implement these J distributions as priors in the gamma-ray analysis. As described in Ref. [35], we use the T-Walk algorithm [55] to compute the full posterior over the 64-dimensional parameter space of dark matter mass, m_χ, and annihilation cross section, $\langle\sigma v\rangle$, along with the J factors and diffuse background normalization parameters of each dSph.

Figure 4 (top) compares the resulting upper limits on the cross section under the different prior assumptions. Limits on $\langle\sigma v\rangle$ are obtained from the posterior distribution conditioned on WIMP mass annihilating to a $b\bar{b}$ final state (in the SM [44], we also show limits for the $\tau^+\tau^-$ channel). Figure 4 (bottom) shows ratios normalized to the limit obtained from the prior (i) above. Satellite priors result in limits that are *weaker* by a factor of between ∼2 and ∼7 than uninformative priors. In particular, under informative priors the thermal relic cross section can only be excluded with 95% probability for $m_\chi \lesssim 40$ GeV at best (and $m_\chi \lesssim 25$ GeV at worst), in contrast to $m_\chi \lesssim 150$ GeV for uninformative priors.

IX. CONCLUSIONS

In this paper, we introduced satellite priors based on physical modeling of dark matter subhalos and a semi-analytical formalism connecting them to the Milky Way's population of satellite galaxies. Our informative priors assign a higher probability to regions of $(\log r_s, \log \rho_s)$ parameter space where subhalos and satellites tend to be found, in contrast to the uniform priors in $(\log r_s, \log \rho_s)$ space widely adopted in the literature. Our priors therefore better reflect the physical mechanisms of subhalo and satellite formation in the cold dark matter picture. When applying our informative satellite priors to the analysis of 11 years of Fermi-LAT data from 31 dSphs, we found that the limits on dark matter annihilation cross section are substantially weaker (between a factor of 2 and 7) compared to using the less informative log-uniform priors. This is a consequence of a systematic shift of most of the J factors to smaller values induced by the informative prior, which downweighs the parameter space region where dSphs are unlikely to form. We conclude that physically motivated priors for the properties of dSphs, which encompass as much as possible our understanding of structure and galaxy formation, are crucial for interpreting the particle properties of dark matter.

ACKNOWLEDGMENTS

This work was supported by Royal Society International Exchanges Scheme between Imperial College London (R. T.) and University of Amsterdam (S. A.), and JSPS/MEXT KAKENHI Grants No. JP17H04836, No. JP18H04578

[2]These are Carina, Draco, Fornax, Leo I, Leo II, Sculptor, Sextans, and Ursa Minor.

(S. A.), No. JP18H04340 (S. A. and N. H.), and No. JP19K23446 (N. H.). A. G. S. and R. T. are supported by Grant No. ST/N000838/1 from the Science and Technology Facilities Council (UK). R. T. was partially supported by a Marie-Skłodowska-Curie RISE (H2020-MSCA-RISE-2015-691164) Grant provided by the European Commission. S. H. gratefully acknowledges funding by the Alexander von Humboldt Foundation and the German Federal Ministry of Education and Research. We acknowledge the UK Materials and Molecular Modelling Hub, which is partially funded by EPSRC (Grant No. EP/P020194/1), and the Imperial College Research Computing Service [63] for providing computational resources. A. G. S. and M. G. W. acknowledge support from NASA's Fermi Guest Investigator Program, Cycle 9, Grant No. NNX16AR33G.

[1] G. Steigman, Cosmology confronts particle physics, Annu. Rev. Nucl. Part. Sci. **29**, 313 (1979).
[2] G. Steigman, B. Dasgupta, and J. F. Beacom, Precise relic WIMP abundance and its impact on searches for dark matter annihilation, Phys. Rev. D **86**, 023506 (2012).
[3] G. Jungman, M. Kamionkowski, and K. Griest, Supersymmetric dark matter, Phys. Rep. **267**, 195 (1996).
[4] L. E. Strigari, Dark matter in dwarf spheroidal galaxies and indirect detection: A review, Rep. Prog. Phys. **81**, 056901 (2018).
[5] M. Walker, *Dark Matter in the Galactic Dwarf Spheroidal Satellites* (Springer Netherlands, Dordrecht, 2013), pp. 1039–1089, https://doi.org/10.1007/978-94-007-5612-0_20.
[6] J. M. Gaskins, A review of indirect searches for particle dark matter, Contemp. Phys. **57**, 496 (2016).
[7] J. D. Simon, The faintest dwarf galaxies, Annu. Rev. Astron. Astrophys. **57**, 375 (2019).
[8] J. F. Navarro, C. S. Frenk, and S. D. M. White, A Universal density profile from hierarchical clustering, Astrophys. J. **490**, 493 (1997).
[9] A. Charbonnier *et al.*, Dark matter profiles and annihilation in dwarf spheroidal galaxies: Prospectives for present and future gamma-ray observatories—I. The classical dwarf spheroidal galaxies, Mon. Not. R. Astron. Soc. **418**, 1526 (2011).
[10] A. Geringer-Sameth, S. M. Koushiappas, and M. Walker, Dwarf galaxy annihilation and decay emission profiles for dark matter experiments, Astrophys. J. **801**, 74 (2015).
[11] V. Bonnivard *et al.*, Dark matter annihilation and decay in dwarf spheroidal galaxies: The classical and ultrafaint dSphs, Mon. Not. R. Astron. Soc. **453**, 849 (2015).
[12] K. Hayashi, K. Ichikawa, S. Matsumoto, M. Ibe, M. N. Ishigaki, and H. Sugai, Dark matter annihilation and decay from non-spherical dark halos in galactic dwarf satellites, Mon. Not. R. Astron. Soc. **461**, 2914 (2016).
[13] G. D. Martinez, A robust determination of Milky Way satellite properties using hierarchical mass modelling, Mon. Not. R. Astron. Soc. **451**, 2524 (2015).
[14] A. Chiappo, J. Cohen-Tanugi, J. Conrad, L. E. Strigari, B. Anderson, and M. A. Sanchez-Conde, Dwarf spheroidal J-factors without priors: A likelihood-based analysis for indirect dark matter searches, Mon. Not. R. Astron. Soc. **466**, 669 (2017).
[15] A. Chiappo, J. Cohen-Tanugi, J. Conrad, and L. Strigari, Dwarf spheroidal J-factor likelihoods for generalized NFW profiles, Mon. Not. R. Astron. Soc. **488**, 2616 (2019).
[16] L. E. Strigari, S. M. Koushiappas, J. S. Bullock, and M. Kaplinghat, Precise constraints on the dark matter content of Milky Way dwarf galaxies for gamma-ray experiments, Phys. Rev. D **75**, 083526 (2007).
[17] J. S. Bullock, T. S. Kolatt, Y. Sigad, R. S. Somerville, A. V. Kravtsov, A. A. Klypin, J. R. Primack, and A. Dekel, Profiles of dark haloes: Evolution, scatter, and environment, Mon. Not. R. Astron. Soc. **321**, 559 (2001).
[18] R. Bartels and S. Ando, Boosting the annihilation boost: Tidal effects on dark matter subhalos and consistent luminosity modeling, Phys. Rev. D **92**, 123508 (2015).
[19] N. Hiroshima, S. Ando, and T. Ishiyama, Modeling evolution of dark matter substructure and annihilation boost, Phys. Rev. D **97**, 123002 (2018).
[20] S. Ando, T. Ishiyama, and N. Hiroshima, Halo substructure boosts to the signatures of dark matter annihilation, Galaxies **7**, 68 (2019).
[21] S. M. Koushiappas, A. R. Zentner, and A. V. Kravtsov, Distribution of annihilation luminosities in dark matter substructure, Phys. Rev. D **82**, 083504 (2010).
[22] S. M. Koushiappas, A. R. Zentner, and T. P. Walker, Observability of gamma rays from neutralino annihilations in the Milky Way substructure, Phys. Rev. D **69**, 043501 (2004).
[23] A. Geringer-Sameth, S. M. Koushiappas, and M. G. Walker, Comprehensive search for dark matter annihilation in dwarf galaxies, Phys. Rev. D **91**, 083535 (2015).
[24] M. Ackermann *et al.* (Fermi-LAT Collaboration), Searching for Dark Matter Annihilation from Milky Way Dwarf Spheroidal Galaxies with Six Years of Fermi Large Area Telescope Data, Phys. Rev. Lett. **115**, 231301 (2015).
[25] J. D. Simon *et al.* (DES Collaboration), Stellar kinematics and metallicities in the ultra-faint dwarf galaxy Reticulum II, Astrophys. J. **808**, 95 (2015).
[26] V. Bonnivard, C. Combet, D. Maurin, A. Geringer-Sameth, S. M. Koushiappas, M. G. Walker, M. Mateo, E. W. Olszewski, and J. I. Bailey III, Dark matter annihilation and decay profiles for the Reticulum II dwarf spheroidal galaxy, Astrophys. J. **808**, L36 (2015).
[27] P. Ullio and M. Valli, A critical reassessment of particle dark matter limits from dwarf satellites, J. Cosmol. Astropart. Phys. 07 (2016) 025.

[28] N. Klop, F. Zandanel, K. Hayashi, and S. Ando, Impact of axisymmetric mass models for dwarf spheroidal galaxies on indirect dark matter searches, Phys. Rev. D **95**, 123012 (2017).
[29] A. Albert *et al.* (DES, Fermi-LAT Collaborations), Searching for dark matter annihilation in recently discovered Milky Way satellites with Fermi-LAT, Astrophys. J. **834**, 110 (2017).
[30] N. W. Evans, J. L. Sanders, and A. Geringer-Sameth, Simple J-factors and D-factors for indirect dark matter detection, Phys. Rev. D **93**, 103512 (2016).
[31] K. K. Boddy, J. Kumar, L. E. Strigari, and M.-Y. Wang, Sommerfeld-enhanced *J*-factors for dwarf spheroidal galaxies, Phys. Rev. D **95**, 123008 (2017).
[32] S. Bergström *et al.*, *J*-factors for self-interacting dark matter in 20 dwarf spheroidal galaxies, Phys. Rev. D **98**, 043017 (2018).
[33] A. B. Pace and L. E. Strigari, Scaling relations for dark matter annihilation and decay profiles in dwarf spheroidal galaxies, Mon. Not. R. Astron. Soc. **482**, 3480 (2019).
[34] M. Petac, P. Ullio, and M. Valli, On velocity-dependent dark matter annihilations in dwarf satellites, J. Cosmol. Astropart. Phys. 12 (2018) 039.
[35] S. Hoof, A. Geringer-Sameth, and R. Trotta, A global analysis of dark matter signals from 27 dwarf spheroidal galaxies using 11 years of Fermi-LAT observations, J. Cosmol. Astropart. Phys. 02 (2020) 012.
[36] K. Boddy, J. Kumar, D. Marfatia, and P. Sandick, Model-independent constraints on dark matter annihilation in dwarf spheroidal galaxies, Phys. Rev. D **97**, 095031 (2018).
[37] F. Calore, P. D. Serpico, and B. Zaldivar, Dark matter constraints from dwarf galaxies: A data-driven analysis, J. Cosmol. Astropart. Phys. 10 (2018) 029.
[38] A. Alvarez, F. Calore, A. Genina, J. I. Read, P. D. Serpico, and B. Zaldivar, Dark matter constraints from dwarf galaxies with data-driven J-factors, arXiv:2002.01229.
[39] J. R. Bond, S. Cole, G. Efstathiou, and N. Kaiser, Excursion set mass functions for hierarchical Gaussian fluctuations, Astrophys. J. **379**, 440 (1991).
[40] X. Yang, H. J. Mo, Y. Zhang, and F. C. v. d. Bosch, An analytical model for the accretion of dark matter subhalos, Astrophys. J. **741**, 13 (2011).
[41] V. Springel, J. Wang, M. Vogelsberger, A. Ludlow, A. Jenkins, A. Helmi, J. F. Navarro, C. S. Frenk, and S. D. M. White, The Aquarius project: The subhaloes of galactic haloes, Mon. Not. R. Astron. Soc. **391**, 1685 (2008).
[42] F. Jiang and F. C. van den Bosch, Statistics of dark matter substructure—I. Model and universal fitting functions, Mon. Not. R. Astron. Soc. **458**, 2848 (2016).
[43] J. Penarrubia, A. J. Benson, M. G. Walker, G. Gilmore, A. McConnachie, and L. Mayer, The impact of dark matter cusps and cores on the satellite galaxy population around spiral galaxies, Mon. Not. R. Astron. Soc. **406**, 1290 (2010).
[44] Please see the Supplemental Material at http://link.aps.org/supplemental/10.1103/PhysRevD.102.061302 for detailed discussions on substructure boost in dSphs, density profiles and *J* factor distributions for each dSph, and WIMP constraints in the case of $\tau^+\tau^-$ annihilation channel.
[45] A. S. Graus, J. S. Bullock, T. Kelley, M. Boylan-Kolchin, S. Garrison-Kimmel, and Y. Qi, How low does it go? Too few Galactic satellites with standard reionization quenching, Mon. Not. R. Astron. Soc. **488**, 4585 (2019).
[46] J. R. Hargis, B. Willman, and A. H. G. Peter, Too many, too few, or just right? The predicted number and distribution of Milky Way dwarf galaxies, Astrophys. J. Lett. **795**, L13 (2014).
[47] B. P. Moster, T. Naab, and S. D. White, Galactic star formation and accretion histories from matching galaxies to dark matter haloes, Mon. Not. R. Astron. Soc. **428**, 3121 (2013).
[48] P. S. Behroozi, R. H. Wechsler, and C. Conroy, The average star formation histories of galaxies in dark matter halos from $z = 0$–8, Astrophys. J. **770**, 57 (2013).
[49] C. Brook, A. Di Cintio, A. Knebe, S. Gottlöber, Y. Hoffman, G. Yepes, and S. Garrison-Kimmel, The stellar-to-halo mass relation for Local Group galaxies, Astrophys. J. Lett. **784**, L14 (2014).
[50] T. Sawala *et al.*, Bent by baryons: The low mass galaxy-halo relation, Mon. Not. R. Astron. Soc. **448**, 2941 (2015).
[51] S. Y. Kim, A. H. G. Peter, and J. R. Hargis, Missing Satellites Problem: Completeness Corrections to the Number of Satellite Galaxies in the Milky Way are Consistent with Cold Dark Matter Predictions, Phys. Rev. Lett. **121**, 211302 (2018).
[52] R. Errani, J. Peñarrubia, and M. G. Walker, Systematics in virial mass estimators for pressure-supported systems, Mon. Not. R. Astron. Soc. **481**, 5073 (2018).
[53] W. B. Atwood *et al.*, The large area telescope on the Fermi Gamma-Ray Space Telescope mission, Astrophys. J. **697**, 1071 (2009).
[54] The Fermi-LAT collaboration, Fermi Large Area Telescope fourth source catalog, arXiv:1902.10045.
[55] G. D. Martinez, J. McKay, B. Farmer, P. Scott, E. Roebber, A. Putze, and J. Conrad, Comparison of statistical sampling methods with ScannerBit, the GAMBIT scanning module, Eur. Phys. J. C **77**, 761 (2017).
[56] F. Calore, I. Cholis, C. McCabe, and C. Weniger, A tale of tails: Dark matter interpretations of the Fermi GeV excess in light of background model systematics, Phys. Rev. D **91**, 063003 (2015).
[57] L. Goodenough and D. Hooper, Possible evidence for dark matter annihilation in the inner Milky Way from the Fermi Gamma Ray Space Telescope, arXiv:0910.2998.
[58] C. Gordon and O. Macias, Dark matter and pulsar model constraints from Galactic Center Fermi-LAT gamma-ray observations, Phys. Rev. D **88**, 083521 (2013); Erratum, Phys. Rev. D **89**, 049901 (2014).
[59] R. Keeley, K. Abazajian, A. Kwa, N. Rodd, and B. Safdi, What the Milky Way's dwarfs tell us about the Galactic Center extended gamma-ray excess, Phys. Rev. D **97**, 103007 (2018).
[60] R. Bartels, S. Krishnamurthy, and C. Weniger, Strong Support for the Millisecond Pulsar Origin of the Galactic Center GeV Excess, Phys. Rev. Lett. **116**, 051102 (2016).

[61] S. K. Lee, M. Lisanti, B. R. Safdi, T. R. Slatyer, and W. Xue, Evidence for Unresolved γ-Ray Point Sources in the Inner Galaxy, Phys. Rev. Lett. **116**, 051103 (2016).

[62] R. K. Leane and T. R. Slatyer, Revival of the Dark Matter Hypothesis for the Galactic Center Gamma-Ray Excess, Phys. Rev. Lett. **123**, 241101 (2019).

[63] https://doi.org/10.14469/hpc/2232.